



# Entropy generation for MHD natural convection in enclosure with a micropolar fluid saturated porous medium with $\text{Al}_2\text{O}_3\text{Cu}$ water hybrid nanofluid\*

A. Mahdy<sup>a</sup>, S.E. Ahmed<sup>b</sup>, M.A. Mansour<sup>c</sup>

<sup>a</sup>Department of Mathematics,  
Faculty of Science, South Valley University,  
Qena, Egypt  
[mahdy@svu.edu.eg](mailto:mahdy@svu.edu.eg)

<sup>b</sup>Department of Mathematics,  
Faculty of Science, King Khalid University,  
Abha 62529, Saudi Arabia  
[sehassan@kku.edu.sa](mailto:sehassan@kku.edu.sa)

<sup>c</sup>Department of Mathematics,  
Faculty of Science, Assiut University,  
Assiut, Egypt  
[mohamed.abdallah5@science.aun.edu.eg](mailto:mohamed.abdallah5@science.aun.edu.eg)

**Received:** October 18, 2020 / **Revised:** March 14, 2021 / **Published online:** November 1, 2021

**Abstract.** This contribution gives a numerical investigation of buoyancy-driven flow of natural convection heat transfer and entropy generation of non-Newtonian hybrid nanofluid ( $\text{Al}_2\text{O}_3\text{-Cu}$ ) within an enclosure square porous cavity. Hybrid nanofluids represent a novel type of enhanced active fluids. During the current theoretical investigation, an actual available empirical data for both thermal conductivity and dynamic viscosity of hybrid nanofluids are applied directly. Numerical simulation have been implemented for solid nanoparticles, the volumetric concentration of which varies from 0.0% (i.e., pure fluid) to 0.1% of hybrid nanofluids. Heat and sink sources are situated on a part of the left and right sides of the cavity with length  $B$ , while the upper and bottom horizontal sides are kept adiabatic. The stated partial differential equations describing the flow are mutated to a dimensionless formulas, then solved numerically via the help of an implicit finite difference approach. The acquired computations are given in terms of streamlines, isotherms, isomicrorotations, isoconcentraions, local Began number, total entropy, local and mean Nusselt numbers. The data illustrates that variations of ratio of the average Nusselt number to the average Nusselt of pure fluid  $Nu_m^+$  is a decreasing function of  $Ha$  and  $\varphi$ , while  $e^+$  is an increasing function of  $Ha$  and  $\varphi$  parameters of hybrid nanofluid.

**Keywords:** entropy, MHD, free convection, hybrid nanofluid, cavity.

---

\*This research was funded by a grant No. R.G.P2/27/42 from the Deanship of Scientific Research at King Khalid University.

## 1 Introduction

Hybrid nanofluids represent another class of nanofluids [17, 27], which can be formed from diverse nanoparticles either in a mixture or in a composite structure distributed in a regular fluid. Hybrid nanofluids can give us working fluids with enhanced chemical and thermophysical features according to a trade-off between the advantages and disadvantages of separated nanoparticles. In particular cases, the nanoparticles can synthesize a nano-composite form in regular fluid, which lead to best thermophysical properties than those predicted from every kind of nanoparticle or its mixture. Nowadays, a number of empirical or numerical investigations have been concerned with hybrid nanofluid as a new technology concept.

Suresh et al. [30] have been measured both the viscosity and thermal conductivity of the  $\text{Al}_2\text{O}_3$ -Cu water hybrid nanofluid with volume fractions from 0.1% to 2%. The data elucidated that both parameters of the hybrid nanofluid enhance with the solid volume nanoparticles concentrations. A numerical investigation has been examined heat transfer in an annulus between two confocal elliptic cylinders filled with Cu- $\text{Al}_2\text{O}_3$  water hybrid nanofluid by Tayebi and Chamkha [32]. Takabi and Salehi [31] numerically addressed natural convection within the laminar regime in a corrugated enclosure in the presence of a discrete heat source on the bottom side wall filled by  $\text{Al}_2\text{O}_3$ -Cu water combined nanofluid. The authors noticed an improvement of the heat transfer rate of  $\text{Al}_2\text{O}_3$ -Cu water hybrid nanofluid compared to those of  $\text{Al}_2\text{O}_3$  water nanofluid when they used the same volume concentration. Devi and Devi [5] exhibited 3-dimensional hybrid nanofluid flow due to a stretching sheet with the impacts of Lorentz force and Newtonian heating within the boundary layer. Sundar et al. [29] formed a MWCNT- $\text{Fe}_3\text{O}_4$  water hybrid nanofluid, whereas a Cu- $\text{TiO}_2$  water hybrid nanofluid has been synthesized by Madhesh et al. [15]. A superb review of hybrid or not nanofluids can be obtained from the paper of Sarkar et al. [28].

In another situation, due to the advancement of engineering expertise and industry, entropy generation represents an appropriate solution to boost efficiency in industrial operations. Bejan presented this concept by means of entropy generation minimization (EGM) [3], which is known as the 2nd law analysis and thermodynamic optimization. Mahdy [18] scrutinized the entropy generation for MHD non-Newtonian tangent hyperbolic nanofluid area adjacent to an accelerating stretched cylinder with variable wall temperature. Entropy analysis of free convection in a split cavity with adiabatic vertical isothermally cooled and horizontal side walls was explored numerically by Famouri and Hooman [6]. They delineated that, as entropy production caused by fluid friction has little effect to total entropy generation, the heat transfer irreversibility boosts with both the Nusselt number and the nondimensional temperature difference. Rashidi et al. [26] considered entropy generation in magneto-hydrodynamic with slip flow due to a rotating porous disk. Entropy generation has been focused by many authors as Ilis et al. [8], Mahdy et al. [19], Ahmed et al. [2], Marzougui et al. [21].

From the other side, natural convection investigation in an enclosure cavity with the impact of a magnetic field is of essential significance in engineering applications according to its ability to govern the fluid flow without physical contact. Of course, for an

electrically conducting fluid flow, the forces of magnetohydrodynamic (MHD) be effective with the existence of an external magnetic field and the Lorentz force interacts with the force of buoyancy in controlling the flow and temperature distributions. Numerical simulation has been given by Ahmed [1] for the convective transport by triangular fins inside an inclined trapezoidal non-Darcy porous cavity that is loaded by a nanofluid. A number of serious contributions [9–12, 24] exhibited natural convection of nanofluids flow inside porous enclosures saturated with a clean fluid as a medium for the heat transfer due to variant boundary conditions. Laouira et al. [14] addressed heat transfer within a horizontal channel with an open trapezoidal cavity associated with a heat source of variable lengths.

The aspect of entropy generation for natural convection of non-Newtonian hybrid nanofluid in a porous cavity has not been investigated well. Hence, in the present comprehensive numerical investigation, a numerical simulation of entropy generation for MHD natural convection heat transfer of  $\text{Al}_2\text{O}_3$ -Cu water non-Newtonian hybrid nanofluid in an enclosure porous square cavity is discussed. Heat and sink sources are situated partially left and right sides of porous square cavity with length  $B$ , whereas the bottom and top horizontal sides remain adiabatic. The originality of this study appears in the following points:

1. Most of the available literature on this topic concerns the heat transfer enhancement using the Newtonian nanofluids and ignores the non-Newtonian nanofluids case, so this study aims to cover this point.
2. Using the suspensions having one more type of the nanoparticles is a modern trend in the computational fluid dynamic field.
3. Examining of the irreversibility process within such kind of domains using the finite differences method is important and interesting for the readers.

## 2 Mathematical modeling

Considered coordinates  $x$  and  $y$  are selected such that  $x$  gives the distance along the bottom horizontal wall, whereas  $y$  gives the distance along the left vertical wall, respectively. Heat and sink sources are located on a part of the left and right walls with length  $B$ . The upper and bottom walls are adiabatic. The hybrid nanofluid used in the analysis is assumed to be incompressible and laminar, and the base fluid (water) and the solid spherical nanoparticles (Cu and  $\text{Al}_2\text{O}_3$ ) are in thermal equilibrium. The thermophysical properties of the base fluid and the nanoparticles are given in Table 1 [11]. The thermophysical properties of the nanofluid are assumed constant except for the density variation, which is determined based on the Boussinesq approximation. Under the above assumptions, the conservation of mass, linear momentum and also conservation of energy equations are given as [25]

$$\frac{\partial u}{\partial x} + \frac{\partial v}{\partial y} = 0, \quad (1)$$

$$\frac{1}{\epsilon^2} \left( u \frac{\partial u}{\partial x} + v \frac{\partial u}{\partial y} \right) = -\frac{1}{\rho_{\text{hnf}}} \frac{\partial \tilde{P}}{\partial x} + \frac{\mu_{\text{hnf}} + k^*}{\rho_{\text{nf}}} \left( \frac{1}{\epsilon} \left( \frac{\partial^2 u}{\partial X^2} + \frac{\partial^2 u}{\partial Y^2} \right) - \frac{u}{K} \right) + \frac{k^*}{\rho_{\text{hnf}}} \frac{\partial \tilde{N}}{\partial y} + \frac{\sigma_{\text{hnf}} B_0^2}{\epsilon \rho_{\text{hnf}}} (v \sin \Phi \cos \Phi - u \sin^2 \Phi), \tag{2}$$

$$\frac{1}{\epsilon^2} \left( u \frac{\partial v}{\partial x} + v \frac{\partial v}{\partial y} \right) = -\frac{1}{\rho_{\text{hnf}}} \frac{\partial \tilde{P}}{\partial y} + \frac{\mu_{\text{hnf}} + k^*}{\rho_{\text{hnf}}} \left( \frac{1}{\epsilon} \left( \frac{\partial^2 v}{\partial X^2} + \frac{\partial^2 v}{\partial Y^2} \right) - \frac{v}{K} \right) + \frac{(\rho\beta)_{\text{hnf}}}{\rho_{\text{hnf}}} g(T - T_c) - \frac{k^*}{\rho_{\text{hnf}}} \frac{\partial \tilde{N}}{\partial x} + \frac{(\rho\beta^*)_{\text{hnf}}}{\rho_{\text{hnf}}} g(C - C_c) + \frac{\sigma_{\text{hnf}} B_0^2}{\epsilon \rho_{\text{hnf}}} (u \sin \Phi \cos \Phi - v \cos^2 \Phi), \tag{3}$$

$$\frac{1}{\epsilon} \left( u \frac{\partial \tilde{N}}{\partial x} + v \frac{\partial \tilde{N}}{\partial y} \right) = \frac{\gamma_{\text{hnf}}}{j \rho_{\text{hnf}}} \left( \frac{\partial^2 \tilde{N}}{\partial x^2} + \frac{\partial^2 \tilde{N}}{\partial y^2} \right) - \frac{2k^*}{j \rho_{\text{hnf}}} \tilde{N} + \frac{k^*}{\epsilon j \rho_{\text{hnf}}} \left( \frac{\partial v}{\partial x} - \frac{\partial u}{\partial y} \right), \tag{4}$$

$$u \frac{\partial T}{\partial x} + v \frac{\partial T}{\partial y} = \alpha_{\text{hnf}} \left( \frac{\partial^2 T}{\partial x^2} + \frac{\partial^2 T}{\partial y^2} \right) + \frac{Q_0}{(\rho c_p)_{\text{hnf}}} (T - T_c) + \frac{\epsilon(\rho c)_p}{(\rho c)_f} \left( D(\nabla C \cdot \nabla T) + \frac{\tilde{D}}{T_c} (\nabla T \cdot \nabla T) \right), \tag{5}$$

$$\frac{1}{\epsilon} \left( u \frac{\partial C}{\partial x} + v \frac{\partial C}{\partial y} \right) = D \left( \frac{\partial^2 C}{\partial x^2} + \frac{\partial^2 C}{\partial y^2} \right) + \frac{\tilde{D}}{T_c} \left( \frac{\partial^2 T}{\partial x^2} + \frac{\partial^2 T}{\partial y^2} \right) - k_c(C - C_c). \tag{6}$$

Through Eqs. (1)–(6),  $x$  and  $y$  are Cartesian coordinates measured along the horizontal and vertical walls of the cavity, respectively.  $u$  and  $v$  are the velocity components along the  $x$ - and  $y$ -axes, respectively.  $T$  is the fluid temperature,  $C$  stands for the concentration,  $\tilde{N}$  is the micro-rotation velocity,  $P$  is the fluid pressure,  $g$  is the gravity acceleration,  $K$  is the permeability, and  $Q_0$  is the volumetric heat generation/absorption rate. Additionally,  $\gamma_{\text{hnf}} = (\mu_{\text{hnf}} + k^*/2)j$  illustrates the spin gradient viscosity,  $j$  and  $k^*$  indicate the micro-inertia density and vortex viscosity, respectively.

The boundary conditions imposed on the flow field are taken as

$$u = v = \tilde{N} = 0, \quad 0 \leq x, y \leq H, \\ \frac{\partial T}{\partial x} = \frac{\partial C}{\partial x} = 0, \quad (D - 0.5B)H \leq y \leq (D + 0.5B)H, \quad \text{and} \\ T = T_h, \quad D \frac{\partial C}{\partial x} + \left( \frac{\tilde{D}}{T_c} \right) \frac{\partial T}{\partial x} = 0, \quad \text{otherwise at walls, } x = 0, H, \tag{7} \\ T = T_c, \quad (D - 0.5B)H \leq x \leq (D + 0.5B)H, \quad \text{and} \\ T = T_h, \quad D \frac{\partial C}{\partial y} + \left( \frac{\tilde{D}}{T_c} \right) \frac{\partial T}{\partial y} = 0, \quad \text{otherwise at walls, } y = 0, H.$$

As previously mentioned, although some literatures studied the determination of thermophysical properties, the classical models are not certain for nanofluids. Of course,

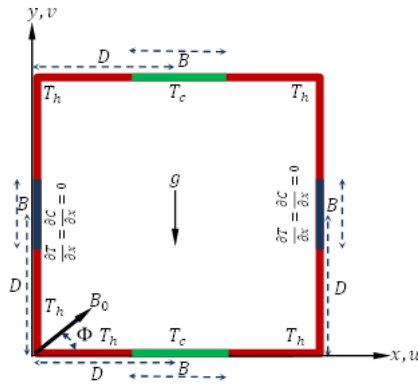


**Figure 1.** Sketch of the geometry and coordinate system of the cavity.

**Table 1.** Thermophysical properties of H<sub>2</sub>O, Cu and Al<sub>2</sub>O<sub>3</sub> [18, 24].

Property	H <sub>2</sub> O	Cu	Al <sub>2</sub> O <sub>3</sub>
$\rho$ (Kg m <sup>-3</sup> )	997.1	8933	3970
$C_p$ (J Kg <sup>-1</sup> K <sup>-1</sup> )	4179	385	765
$k$ (W m <sup>-1</sup> K <sup>-1</sup> )	0.613	401	40
$\beta \cdot 10^5$ (K <sup>-1</sup> )	21	1.67	0.85
$\sigma$ (S m <sup>-1</sup> )	0.05	$5.96 \cdot 10^7$	$10^{-10}$

experimental results allow us to select an appropriate model for a specified property. The effective properties of the Al<sub>2</sub>O<sub>3</sub>-water and Cu-water nanofluid are defined as follows [9]:

$$\rho_{nf} = (1 - \varphi)\rho_{bf} + \varphi\rho_p, \tag{8}$$

Equation (8) was originally introduced for determining density of nanofluid and then widely employed in [9]. So, the density of hybrid nanofluid is specified by

$$\rho_{hnf} = \varphi_{Al_2O_3}\rho_{Al_2O_3} + \varphi_{Cu}\rho_{Cu} + (1 - \varphi)\rho_{bf},$$

where  $\varphi$  is the overall volume concentration of two different types of nanoparticles dispersed in hybrid nanofluid and is calculated as  $\varphi = \varphi_{Al_2O_3} + \varphi_{Cu}$ , and the heat capacitance of the nanofluid given is by Khanafer et al. [12] as

$$(\rho C_p)_{nf} = \varphi(\rho C_p)_p + (1 - \varphi)(\rho C_p)_{bf},$$

According to Eq. (8), heat capacity of hybrid nanofluid can be determined by follows:

$$(\rho C_p)_{hnf} = \varphi_{Al_2O_3}(\rho C_p)_{Al_2O_3} + \varphi_{Cu}(\rho C_p)_{Cu} + (1 - \varphi)(\rho C_p)_{bf}.$$

The thermal expansion factor of the nanofluid can be determined by

$$(\rho\beta)_{nf} = \varphi(\rho\beta)_p + (1 - \varphi)(\rho\beta)_{bf}, \tag{9}$$

where  $\beta_{bf}$  and  $\beta_p$  are the coefficients of thermal expansion of the fluid and of the solid fractions, respectively. Hence, for hybrid nanofluid, thermal expansion can be defined as follows:

$$(\rho\beta)_{hnf} = \varphi_{Al_2O_3}(\rho\beta)_{Al_2O_3} + \varphi_{Cu}(\rho\beta)_{Cu} + (1 - \varphi)(\rho\beta)_{bf}.$$

Thermal diffusivity of the nanofluid,  $\alpha_{nf}$ , is given by Oztop and Abu-Nada [24] as

$$\alpha_{nf} = \frac{k_{nf}}{(\rho C_p)_{nf}},$$

In Eq. (9),  $k_{nf}$  is the thermal conductivity of the nanofluid, which for spherical nanoparticles referring to the Maxwell–Garnetts model [22], is

$$\frac{k_{nf}}{k_{bf}} = \frac{(k_p + 2k_{bf}) - 2\varphi(k_{bf} - k_p)}{(k_p + 2k_{bf}) + \varphi(k_{bf} - k_p)}. \tag{10}$$

Thus, thermal diffusivity of the hybrid nanofluid,  $\alpha_{hnf}$ , can be defined as

$$\alpha_{hnf} = \frac{k_{hnf}}{(\rho C_p)_{hnf}}.$$

If the thermal conductivity of hybrid nanofluid is defined according to Maxwell model, Eq. (10) must be employed for this objective:

$$\frac{k_{hnf}}{k_{bf}} = \frac{\left(\frac{\varphi_1 k_1 + \varphi_2 k_2}{\varphi} + 2k_{bf} + 2(\varphi_1 k_1 + \varphi_2 k_2) - 2\varphi k_{bf}\right)}{\left(\frac{\varphi_1 k_1 + \varphi_2 k_2}{\varphi} + 2k_{bf} - (\varphi_1 k_1 + \varphi_2 k_2) + \varphi k_{bf}\right)}.$$

Note ( $Al_2O_3 \equiv \varphi_1$ ,  $Cu \equiv \varphi_2$ ), the effective dynamic viscosity of the nanofluid based on the Brinkman model [4] is expressed as

$$\mu_{nf} = \frac{\mu_{bf}}{(1 - \varphi)^{2.5}},$$

where  $\mu_{bf}$  is the viscosity of the fluid fraction, then the effective dynamic viscosity of the hybrid nanofluid is

$$\mu_{hnf} = \frac{\mu_{bf}}{(1 - \varphi_1)^{5/2}(1 - \varphi_2)^{5/2}},$$

and the effective electrical conductivity of nanofluid was employed by Maxwell [22] as

$$\frac{\sigma_{nf}}{\sigma_{bf}} = 1 + \frac{3\left(\frac{\sigma_p}{\sigma_{bf}} - 1\right)\varphi}{\left(\frac{\sigma_p}{\sigma_{bf}} + 2\right) - \left(\frac{\sigma_p}{\sigma_{bf}} - 1\right)\varphi},$$

and the effective electrical conductivity of hybrid nanofluid is

$$\frac{\sigma_{hnf}}{\sigma_{bf}} = 1 + \frac{3\left(\frac{\varphi_1 \sigma_1 + \varphi_2 \sigma_2}{\sigma_{bf}} - (\varphi_1 + \varphi_2)\right)}{\left(\frac{\varphi_1 \sigma_1 + \varphi_2 \sigma_2}{\varphi \sigma_{bf}} + 2\right) - \left(\frac{\varphi_1 \sigma_1 + \varphi_2 \sigma_2}{\sigma_{bf}} - (\varphi_1 + \varphi_2)\right)}.$$

Introducing the following dimensionless set

$$\begin{aligned}
 X &= \frac{x}{H}, & Y &= \frac{y}{H}, & U &= \frac{uH}{\alpha_f}, & V &= \frac{vH}{\alpha_f}, & P &= \frac{\tilde{P}H^2}{\rho_f \alpha_f^2}, \\
 \theta &= \frac{T - T_c}{\Delta T}, & \phi &= \frac{C - C_c}{\Delta C}, & N &= \frac{H^2}{\alpha_f} \tilde{N}, & \Delta T &= T_h - T_c, \\
 \Delta C &= C_h - C_c, & Q &= \frac{Q_0 H^2}{(\rho C_p)_f \alpha_f}, & T_0 &= \frac{T_h + T_c}{2}, & \chi &= \frac{H^2}{j}, \\
 D &= \frac{d}{H}, & B &= \frac{b}{H}, & Nt &= \frac{\delta \Delta T \tilde{D}}{T_c \alpha_f}, & Nb &= \frac{\delta D \Delta C}{\alpha_f}
 \end{aligned} \tag{11}$$

into Eqs. (1)–(7) yields the following dimensionless equations:

$$\begin{aligned}
 \frac{\partial U}{\partial X} + \frac{\partial V}{\partial Y} &= 0, \\
 \frac{1}{\epsilon^2} \frac{\rho_{\text{hnf}}}{\rho_f} \left( U \frac{\partial U}{\partial X} + V \frac{\partial U}{\partial Y} \right) &= -\frac{\rho_{\text{hnf}}}{\rho_h} \frac{\partial P}{\partial X} - \frac{Pr}{Da} \left( \frac{\mu_{\text{hnf}}}{\mu_f} + k \right) U \\
 &\quad + \frac{\sigma_{\text{hnf}}}{\epsilon \sigma_f} Ha^2 Pr (V \sin \Phi \cos \Phi - U \sin^2 \Phi) \\
 &\quad + \frac{Pr}{\epsilon} \left( \frac{\mu_{\text{hnf}}}{\mu_f} + k \right) \left( \frac{\partial^2 U}{\partial X^2} + \frac{\partial^2 U}{\partial Y^2} \right) + k Pr \frac{\partial N}{\partial Y}, \\
 \frac{1}{\epsilon^2} \left( U \frac{\partial V}{\partial X} + V \frac{\partial V}{\partial Y} \right) &= -\frac{\partial P}{\partial Y} + \frac{Pr}{\epsilon} \frac{\rho_f}{\rho_{\text{nf}}} \left( \frac{\mu_{\text{hnf}}}{\mu_f} + k \right) \left( \frac{\partial^2 V}{\partial X^2} + \frac{\partial^2 V}{\partial Y^2} \right) \\
 &\quad - k Pr \frac{\rho_f}{\rho_{\text{hnf}}} \frac{\partial N}{\partial X} - \frac{Pr}{Da} \frac{\rho_f}{\rho_{\text{hnf}}} \left( \frac{\mu_{\text{hnf}}}{\mu_f} + k \right) V \\
 &\quad + Pr Ra \frac{(\rho\beta)_{\text{hnf}}}{\rho_{\text{hnf}} \beta_f} \theta + Ra_c \phi \\
 &\quad + \frac{\rho_f}{\rho_{\text{hnf}}} \frac{\sigma_{\text{hnf}}}{\epsilon \sigma_f} Ha^2 Pr (U \sin \Phi \cos \Phi - V \cos^2 \Phi), \\
 \frac{\rho_{\text{hnf}}}{\epsilon \rho_f} \left( U \frac{\partial N}{\partial X} + V \frac{\partial N}{\partial Y} \right) &= Pr \left( \frac{\mu_{\text{hnf}}}{\mu_f} + \frac{k}{2} \right) \left( \frac{\partial^2 N}{\partial X^2} + \frac{\partial^2 N}{\partial Y^2} \right) \\
 &\quad - k Pr \chi \left( 2N - \frac{1}{\epsilon} \left( \frac{\partial V}{\partial X} - \frac{\partial U}{\partial Y} \right) \right), \\
 U \frac{\partial \theta}{\partial X} + V \frac{\partial \theta}{\partial Y} &= \frac{\alpha_{\text{hnf}}}{\alpha_f} \left( \frac{\partial^2 \theta}{\partial X^2} + \frac{\partial^2 \theta}{\partial Y^2} \right) + \nabla \theta (Nb \nabla \phi + Nt \nabla \theta) \\
 &\quad + \frac{(\rho c_p)_f}{(\rho c_p)_{\text{hnf}}} Q \theta, \\
 \frac{1}{\epsilon} \left( U \frac{\partial \phi}{\partial X} + V \frac{\partial \phi}{\partial Y} \right) &= \frac{Pr}{Sc} \left( \frac{\partial^2 g(\phi + N_c \theta)}{\partial X^2} + \frac{\partial^2 (\phi + N_c \theta)}{\partial Y^2} \right) - Kr Pr \phi,
 \end{aligned}$$

wherein

$$Pr = \frac{\nu_f}{\alpha_f}, \quad Ra = \frac{g\beta_f H^3 \Delta T}{\nu_f \alpha_f}, \quad Ra_c = \frac{(\rho\beta^*)_f g H^3 \Delta C}{\rho_f \alpha_f^2}, \quad Ha = B_0 H \sqrt{\frac{\sigma_f}{\mu_f}},$$

$$Sc = \frac{\nu_f}{D}, \quad N_C = \frac{\tilde{D} \Delta T}{D \Delta C}, \quad k = \frac{k^*}{\mu_f}, \quad Da = \frac{K}{H^2}, \quad Kr = \frac{k_c H^2}{\nu_f}.$$

The boundary conditions now take the following formula:

$$U = V = N = 0 \quad 0 \leq X, y \leq 1,$$

$$\frac{\partial \theta}{\partial X} = \frac{\partial \phi}{\partial X} = 0, \quad D - 0.5B \leq Y \leq D + 0.5B, \quad \text{and}$$

$$\theta = 1.0, \quad \frac{\partial \phi}{\partial X} + \left(\frac{Nt}{Nb}\right) \frac{\partial \theta}{\partial X} = 0, \quad \text{otherwise at walls, } X = 0, 1,$$

$$\theta = 0, \quad D - 0.5B \leq X \leq D + 0.5B, \quad \text{and}$$

$$\theta = 1.0, \quad \frac{\partial \phi}{\partial Y} + \left(\frac{Nt}{Nb}\right) \frac{\partial \theta}{\partial Y} = 0, \quad \text{otherwise at walls, } Y = 0, 1.$$

The local Nusselt numbers are given by

$$Nu_X = -\frac{k_{\text{hnf}}}{k_f} \left(\frac{\partial \theta}{\partial X}\right)_{X=0,1} \quad \text{and} \quad Nu_Y = -\frac{k_{\text{hnf}}}{k_f} \left(\frac{\partial \theta}{\partial Y}\right)_{Y=0,1},$$

and the average Nusselt numbers are given by

$$(Nu_m)_{X=0,1} = \frac{2}{1-B} \int_0^{0.5-0.5B} Nu_{X=0,1} dX, \quad \frac{2}{1-B} \int_{0.5+0.5B}^1 Nu_{X=0,1} dX,$$

$$(Nu_m)_{Y=0,1} = \frac{2}{1-B} \int_0^{0.5-0.5B} Nu_{Y=0,1} dY, \quad \frac{2}{1-B} \int_{0.5+0.5B}^1 Nu_{Y=0,1} dY,$$

$$Nu_m = \frac{(Nu_m)_{Y=0,1} + (Nu_m)_{X=0,1}}{8}.$$

### 3 Entropy generation analysis

Due to Mahmud and Fraser [20], Magherbi et al. [16] and local thermodynamic equilibrium of linear transport theory, the nondimensional total local entropy generation can be

expressed by implementing the dimensionless variables appeared in Eq. (11) as

$$\begin{aligned}
 S &= \tilde{S} \frac{H^2 T_0^2}{k_f \Delta T^2} \\
 &= \frac{k_{nf}}{k_f} \left\{ \left( \frac{\partial \theta}{\partial X} \right)^2 + \left( \frac{\partial \theta}{\partial Y} \right)^2 \right\} \\
 &\quad + \tilde{\varphi}_1 \left( \frac{\mu_{nf}}{\mu_f} + K \right) \left\{ \frac{1}{Da} (U^2 + V^2) + 2 \left\{ \left( \frac{\partial U}{\partial X} \right)^2 + \left( \frac{\partial V}{\partial Y} \right)^2 \right\} + \left( \frac{\partial V}{\partial X} + \frac{\partial U}{\partial Y} \right)^2 \right\} \\
 &\quad + \tilde{\varphi}_2 \left\{ \left( \frac{\partial \phi}{\partial X} \right)^2 + \left( \frac{\partial \phi}{\partial Y} \right)^2 \right\} + \tilde{\varphi}_3 \left\{ \frac{\partial \phi}{\partial X} \frac{\partial \theta}{\partial X} + \frac{\partial \phi}{\partial Y} \frac{\partial \theta}{\partial Y} \right\} \\
 &\quad + \tilde{\varphi}_1 \frac{\sigma_{nf}}{\sigma_f} Ha^2 Re^2 Pr^2 (U \sin \Phi - V \cos \Phi)^2 \\
 &= S_h + S_v + S_\phi + S_{\phi,\theta} + S_j.
 \end{aligned}$$

Here the irreversibility ratios  $\tilde{\varphi}_1$ ,  $\tilde{\varphi}_2$  and  $\tilde{\varphi}_3$  can be expressed by

$$\varphi_1 = \frac{\mu_f T_0}{k_f} \left( \frac{\alpha_f}{\Delta T H} \right)^2, \quad \varphi_2 = \frac{RD}{C_0 k_f} \left( \frac{T_0 \Delta C}{\Delta T} \right)^2, \quad \varphi_3 = RD \frac{T_0 \Delta C}{k_f \Delta T}.$$

Here the local Bejan number is defined as in Oueslati et al. [23]:

$$Be = \frac{S_h + S_\phi + S_{\phi,\theta}}{S}.$$

For obtaining the impact of nanoparticles, magnetic field and difference of temperature on the average Nusselt number, total entropy generation and Bejan number, the following ratio of the average Nusselt number to the average Nusselt to the pure fluid  $Nu_m^+$ , ratio of the average Nusselt number to the average Nusselt number to a horizontal magnetic field  $Nu_m^{++}$ , ratio of the entropy generation to the entropy generation to the pure fluid  $S^+$ , ratio of the entropy generation to the entropy generation to a horizontal magnetic field  $S^{++}$ , ratio of the average Bejan number to the average Bejan number to the pure fluid  $Be^+$ , ratio of the average Bejan number to the average Bejan number to a horizontal magnetic field  $Be^{++}$ , ratio of the entropy generation ratio to the average Nusselt ratio to the pure fluid  $e^+$ , ratio of the entropy generation ratio to the average Nusselt ratio to a horizontal magnetic field  $e^{++}$  are stated as

$$\begin{aligned}
 Nu_m^+ &= \frac{Nu_m}{(Nu_m)_{\varphi=0}} \quad \text{and} \quad Nu_m^{++} = \frac{Nu_m}{(Nu_m)_{\Phi=0^0}}, \\
 S^+ &= \frac{S}{(S)_{\varphi=0}} \quad \text{and} \quad S^{++} = \frac{S}{(S)_{\Phi=0^0}}, \\
 Be^+ &= \frac{Be}{(Be)_{\varphi=0}} \quad \text{and} \quad Be^{++} = \frac{Be}{(Be)_{\Phi=0^0}}, \\
 e^+ &= \frac{S^+}{Nu_m^+} \quad \text{and} \quad e^{++} = \frac{S^{++}}{Nu_m^{++}}.
 \end{aligned}$$

### 4 Numerical technique and validation

The governing equations are solved numerically using FDM (finite difference method). The first point in the solution methodology is writing the previous system in the following general form:

$$U \frac{\partial \Omega}{\partial X} + V \frac{\partial \Omega}{\partial Y} = \Gamma_{\Omega} \left[ \frac{\partial^2 \Omega}{\partial X^2} + \frac{\partial^2 \Omega}{\partial Y^2} \right] + S_{\Omega}.$$

Here it should be mentioned that  $S_{\Omega}$  refers to the source terms (including the pressure gradients and buoyancy terms in the momentum equations). The central differences scheme is used to estimate the first and second derivatives as

$$\frac{\partial \Omega}{\partial X} = \frac{\Omega_{i+1,j} - \Omega_{i-1,j}}{X_{i+1} - X_{i-1}}, \quad \frac{\partial \Omega}{\partial Y} = \frac{\Omega_{i,j+1} - \Omega_{i,j-1}}{Y_{j+1} - Y_{j-1}}, \tag{12}$$

$$\frac{\partial^2 \Omega}{\partial X^2} + \frac{\partial^2 \Omega}{\partial Y^2} = \frac{\Omega_{i+1,j} - 2\Omega_{i,j} + \Omega_{i-1,j}}{(\Delta X)^2} + \frac{\Omega_{i,j-1} - 2\Omega_{i,j} + \Omega_{i,j+1}}{(\Delta Y)^2}. \tag{13}$$

In Eqs. (12)–(13),  $\Omega$  refers to the dependent variables  $U, V, N$  and  $\theta$  and  $\Delta X = X_{i+1} - X_i, \Delta Y = Y_{j+1} - Y_j$ . Using the previous forms, the following algebraic system is obtained:

$$A_p \Omega_{i,j} = A_E \Omega_{i+1,j} + A_W \Omega_{i-1,j} + A_N \Omega_{i,j+1} + A_S \Omega_{i,j-1} + S_p. \tag{14}$$

The algebraic system (14) is solved using SUR (successive under relaxation method) with the relaxation parameter  $\alpha^* = 0.8$ . The suitable grid size for all computations is found to be  $81 \times 81$ . This section is due to the grid independency study, which is performed and presented in Table 2. Additionally, a validation test is performed and presented in Table 3. This test includes comparisons of the average Nusselt number with the results earned by Kim et al. [13] for variations of the Rayleigh number  $Ra$ . The table disclosed that the relative error in the results is ranging between 2.26% and  $-3.86\%$ , which confirm the accuracy of the present results. Other comparisons are performed and presented in Table 4. In this table, maximum values of the stream function  $\psi_{\max}$  and temperature  $\theta_{\max}$  for various values of the Hartmann number  $Ha$  and magnetic field inclination angle  $\Phi$  are compared with those of Grosan et al. [7]. The results indicate to a very good agreement between the results is found.

**Table 2.** Grid independency study at  $Ra = 10^5, Da = 10^{-3}, Nb = 0.4, Nt = 0.3, \varphi = 5\%, B = D = 0.5, \Phi = 45^\circ, Ha = 10$ .

Grid size	$Nu_m$	Grid size	$Nu_m$
$31 \times 31$	1.53745	$81 \times 81$	1.67429
$41 \times 41$	1.63117	$101 \times 101$	1.71653
$61 \times 61$	1.67995	$121 \times 121$	1.71687

**Table 3.** Comparison of the surface-averaged Nusselt number at the side wall when  $Pr = 0.71$ .

$Ra$	Present results	Kim et al. [13]	Difference (%)
$10^3$	1.6847	1.6220	-3.86
$10^4$	1.6966	1.6905	-0.36
$10^5$	2.0212	2.0679	2.26

**Table 4.** Comparisons of the maximum values of the stream function and temperature for various values of  $Ha$  and  $\Phi$  at  $Ra = 10^3$ .

$Ha$	$\Phi$	Grosan et al. [7]		Present results	
		$\psi_{max}$	$\theta_{max}$	$\psi_{max}$	$\theta_{max}$
0	0	3.3560	0.0985	3.5338	0.09735
1	0	2.3451	0.1131	2.4677	0.11189
1	$\pi/6$	2.4665	0.1114	2.5867	0.11026
1	$\pi/4$	2.6236	0.1095	2.7473	0.10832
1	$\pi/2$	3.1418	0.1048	3.2759	0.10343

### 5 Results and discussion

At this point of the analysis, a comprehensive set of graphical simulation computations through Figs. 2–10 are delineated to clarify the impacts of different controlling physical parameters on the hydrodynamic and thermal behavior of non-Newtonian hybrid nanofluid ( $Al_2O_3-Cu$ ) in an enclosure porous square cavity with impact of Lorentz force. Streamlines, isomicrorotations, isotherms, isoconcentraions, local Began number, local and average Nusselt numbers represent the visualization instruments utilized for the numerical computations. Given results are calculated for wide ranges of the controlling parameters, that is,  $0.2 \leq B \leq 0.8$ ,  $0.1 \leq k \leq 0.4$ ,  $-8 \leq Q \leq 8$ ,  $0.2 \leq \epsilon \leq 0.8$ ,  $0.1 \leq Nt \leq 5.0$ ,  $0.005 \leq Nb \leq 0.6$ ,  $10^{-7} \leq Da \leq 10^{-2}$  and  $0 \leq Ha \leq 200$ , where we chose that  $D = 0.5$ ,  $Kr = 0.05$ ,  $k = 1.0$ ,  $Sc = 1.0$ ,  $N_C = 1.0$ ,  $Da = 10^{-3}$ ,  $Ra = 10^3$ ,  $Ra_c = 10$ ,  $N_b = 0.4$ ,  $N_t = 0.3$ ,  $\epsilon = 0.5$ ,  $\Phi = \pi/4$ ,  $B = 0.5$ ,  $\varphi_{Al_2O_3} = \varphi_{Cu} = 0.025$  and  $Q = 1$  to be fixed parameters when we search the effect of any of governing parameters.

Figure 2 shows contours of the streamlines, isotherms, angular velocity, isoconcentration and local Began number for variations of the vortex viscosity parameter ( $0.1 \leq k \leq 0.4$ ). The figure discloses that two symmetrical eddies are formulated within the enclosure for all values of  $k$ . In addition, the increase in  $k$  results in a weakness in the nanofluid flows. The isotherms show thermal zones near the heated parts, and the temperatures distribute in the entire domain indicating a decrease in the thermal boundary layer as  $k$  is increased. Further, because of the source terms in the angular velocity equation, contours of the angular velocity follow the behavior of the streamlines. The angular velocity displays symmetrical features within the domain accompanied by an enhancement in the angular velocity as the vortex parameter is increased. The isoconcentrations show that the negative values of the nanoparticles are occurred near the heated parts, while the positive values near the cold parts. In all cases, variations of  $k$  have no a significant effects on distributions or values of the concentration. Contours of the local Began number indicate

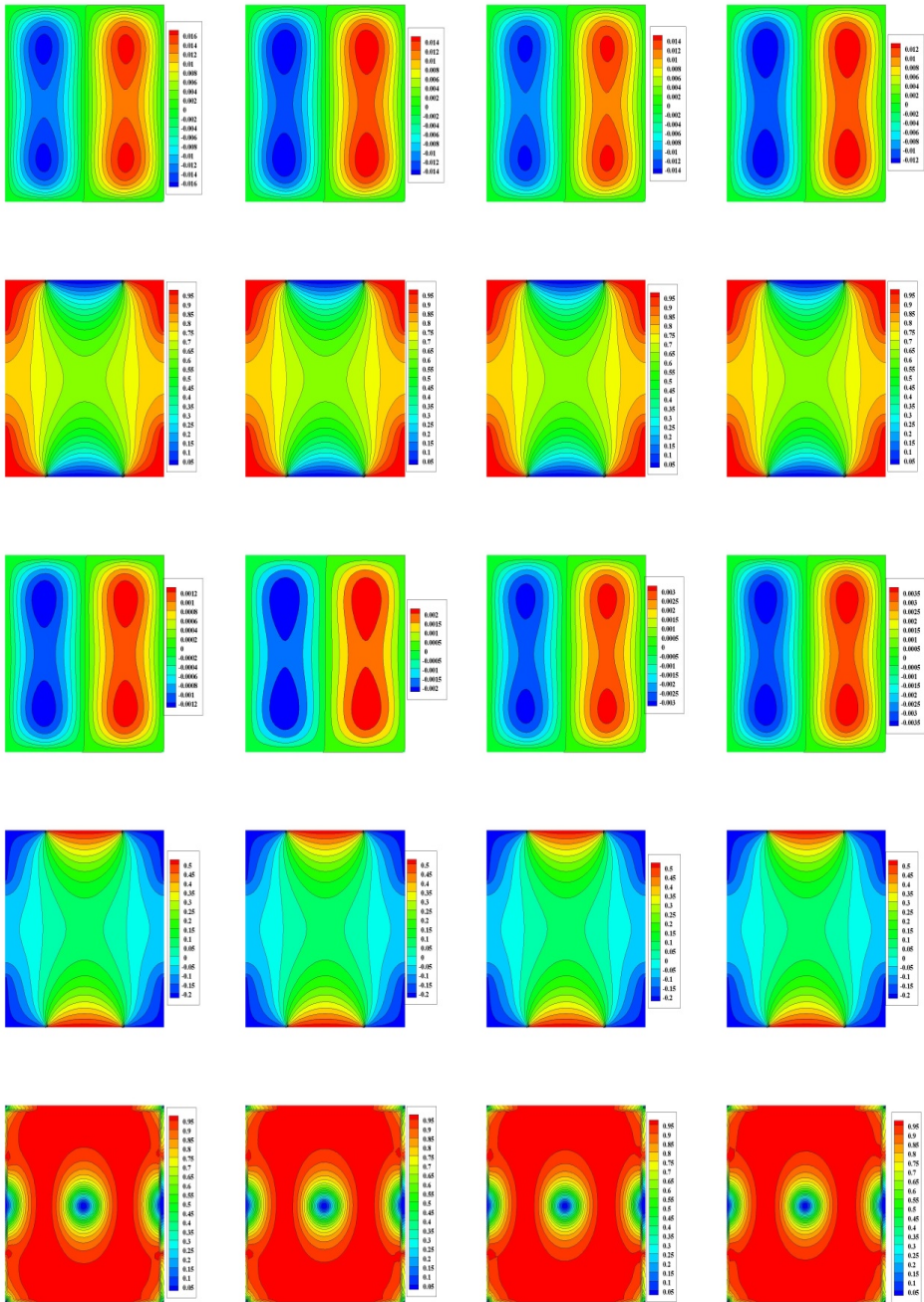
to the local irreversibilities due to the thermal gradients are smalls near the adiabatic parts and at the center of the flow domain, while the local irreversibilities due to the thermal gradients are dominance in the remaining area. All these mentioned behaviors are due to the dynamic viscosity of the mixture, which increases as  $k$  is increased.

Figure 3 depicts features of the streamlines, isotherms, isomicrorotation, isoconcentration and local Began number for variations of the Darcy number at  $\varphi = 0.05$ ,  $k = 0.5$ ,  $B = 0.5$ ,  $\Phi = 45^\circ$ ,  $Q = 1$ ,  $\epsilon = 0.5$ ,  $Nb = 0.4$ ,  $Nt = 0.3$ . It is noted that symmetrical features are earned for both the streamlines and the angular velocity. Additionally, deactivation in the nanofluid motion, as well as suppression in the angular velocity, are obtained as  $Da$  is decreased. This behavior is explained with the permeability of the porous medium that decreases as  $Da$  is decreased, which slowdown the flows. The isotherms and the isoconcentration show a decrease in the thermal and concentration boundary layers as  $Da$  decreases indicating a low heat transfer in these cases. Contours of the local Began number demonstrate that the local irreversibilities due to gradients of the temperature are increased as  $Da$  decreases. Constantly decreasing the number of Darcy produces that the temperature gradients irreversibilities dominate on the entire area.

Figure 4 exhibits contours of the streamlines, isotherms, isomicrorotation, isoconcentration and local Began number for variations of lengths of the heated parts  $B$  at  $\varphi = 0.05$ ,  $k = 0.5$ ,  $\Phi = 45^\circ$ ,  $Q = 1$ ,  $Da = 10^{-3}$ ,  $\epsilon = 0.5$ ,  $Nb = 0.4$ ,  $Nt = 0.3$ . Here it should be mentioned that the increase in  $B$  leads to the increase in the cold and adiabatic parts. Features of the streamlines and the angular velocity show that the increase in  $B$  to 0.6 enhances the flow of the mixture, while more increase in  $B$  causes a weakness in the nanofluid flow. In addition, large thermal zones are obtained near the domain boundaries at small values of  $B$ . However, the increase in  $B$  causes that a large cold zone is formulated nears the horizontal walls. The isoconcentrations exhibit that there are no any negative values of the concentration at small values of  $B$ . On the contrary, the negative values of the concentration are increased as  $B$  is increased. Finally, the increase in  $B$  causes that the local irreversibilities due to the temperature gradients increase, particularly, near the boundaries, while the local irreversibilities due to the fluid friction are limited near the adiabatic parts and at the center of the enclosure.

Figures 5(a) and 5(b) illustrate impacts of lengths of the active parts  $B$  on the local Nusselt number  $Nu_s$  along the horizontal walls and the ratio of the entropy generation ratio to the average Nusselt ratio at a horizontal magnetic field  $e^{++}$  at  $k = 0.5$ ,  $\Phi = 45^\circ$ ,  $Q = 1$ ,  $Da = 10^{-3}$ ,  $\epsilon = 0.5$ ,  $Nb = 0.4$ ,  $Nt = 0.3$ . It is remarkable that the increase in  $B$  enhances gradients of the temperature, and hence, the rate of the heat transfer is enhanced. In addition, the increase in  $B$  enhances the ratio of the entropy generation ratio to the average Nusselt ratio at a horizontal magnetic field  $e^{++}$  due to the increase in the thermal boundary layers.

Figures 6(a) and 6(b) display profiles ratio of the average Nusselt number to the average Nusselt number at a horizontal magnetic field  $Nu_m^{++}$  and ratio of the entropy generation ratio to the average Nusselt ratio at a horizontal magnetic field  $e^{++}$  under effects of the vortex viscosity  $k$ . A clear reduction in values of  $Nu_m^{++}$  is obtained as  $k$  is increased due to the increase in the overall dynamic viscosity of the mixture. On the contrary, value of  $e^{++}$  is supported as  $k$  is grown due to the inverse relation between  $e^{++}$



**Figure 2.** Contours of streamlines, isotherms, isomicrorotation, isoconcentration and local Began number (from top to bottom) for variations of the vortex-viscosity parameter  $k = 0.1, 0.2, 0.3$  and  $0.4$  (from left to right).

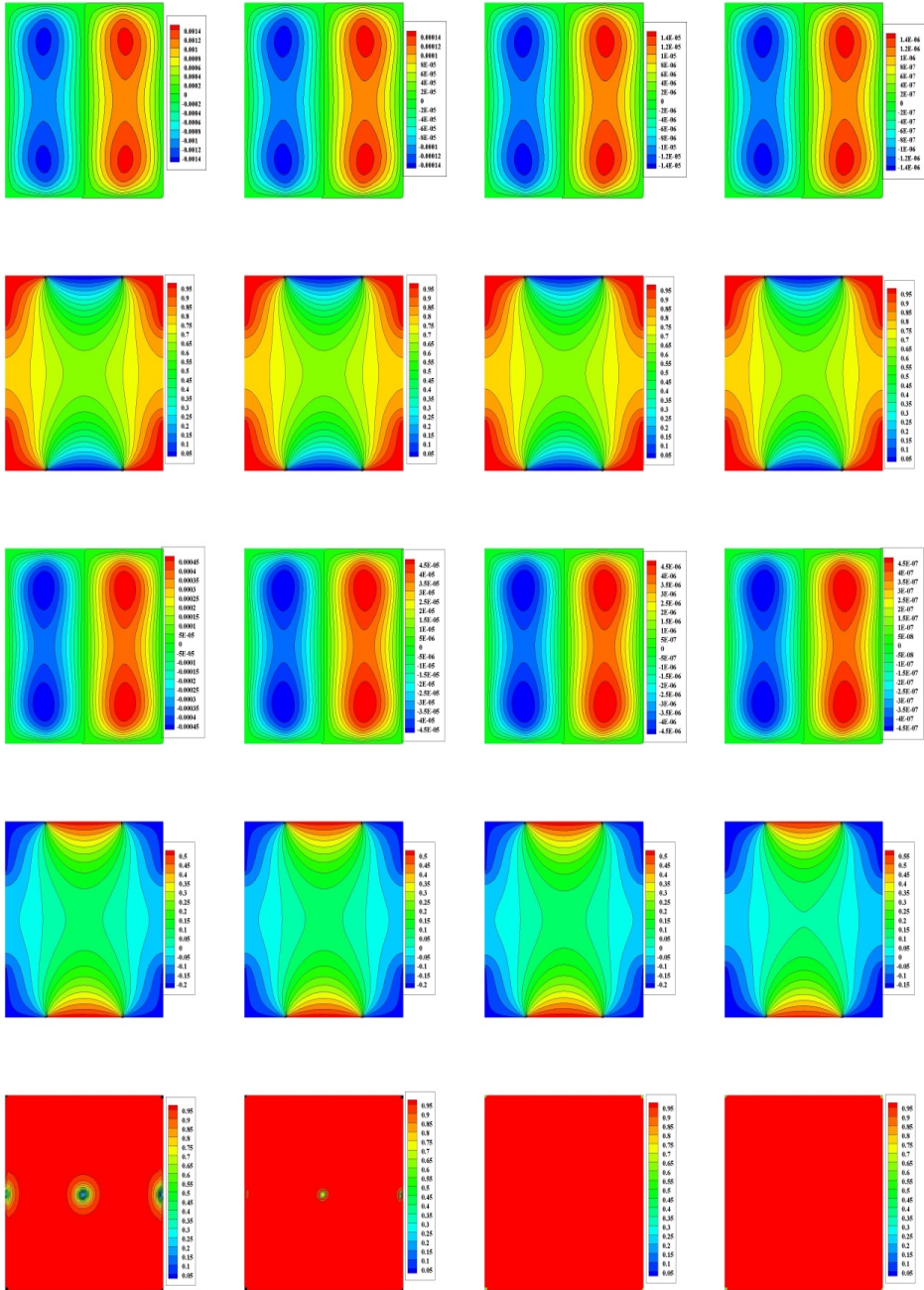
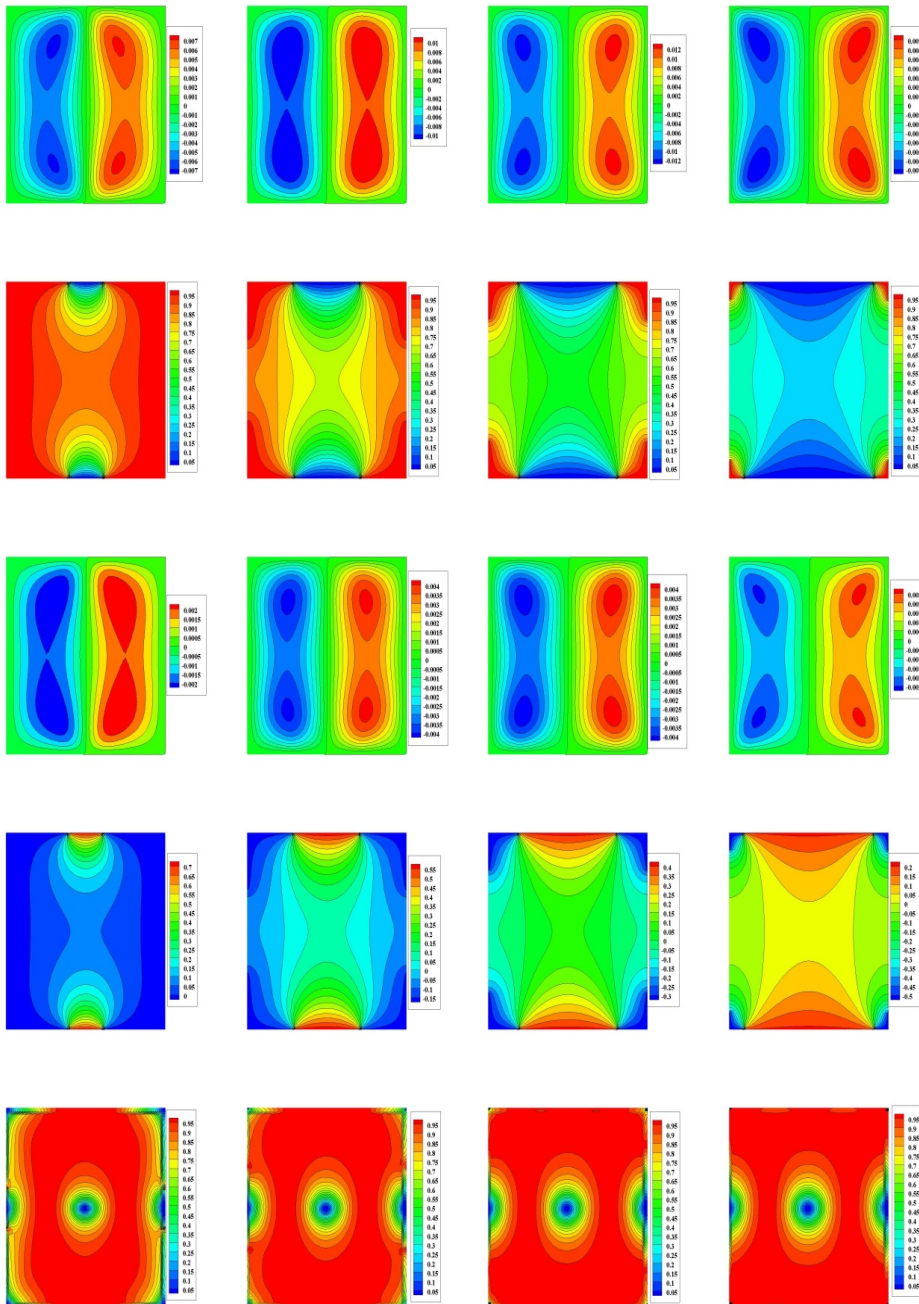


Figure 3. Contours of streamlines, isotherms, isomicrorotation, isoconcentration and local Began number (from top to bottom) for variations of the Darcy number  $Da = 10^{-4}, 10^{-5}, 10^{-6}$  and  $10^{-7}$  (from left to right).



**Figure 4.** Contours of streamlines, isotherms, isomicrorotation, isoconcentration and local Began number (from top to bottom) for variations of lengths of the active parts  $B = 0.2, 0.4, 0.6$  and  $0.8$  (from left to right).

and  $Nu_m^{++}$ . The results also indicated that value of  $Nu_m^{++}$  takes its minimum in case of a horizontal magnetic field ( $\Phi = 0, 180^\circ, 360^\circ$ ), while  $e^{++}$  takes the opposite features.

Figures 7(a), 7(b) and 8(a) expose profiles of ratio of the average Nusselt number to the average Nusselt at the pure fluid  $Nu_m^+$ , ratio of the average Nusselt number to the average Nusselt number at a horizontal magnetic field  $Nu_m^{++}$  and ratio of the entropy generation ratio to the average Nusselt ratio at a horizontal magnetic field  $e^{++}$  for variations of heat generation/absorption parameter  $Q$ . It is noteworthy that  $Nu_m^+$  is enhanced as  $Q$  is grown due to the increase in the temperature differences within the geometry. However,  $Nu_m^{++}$  is significantly reduced as  $Q$  increases, also, as mentioned previously, because of the inverse relation between  $e^{++}$  and  $Nu_m^{++}$ . Figure 8(a) shows a clear support in values of  $e^{++}$  as  $Q$  is enhanced. The physical interpretation of this behavior is due to the extra heat generation in the flow domain as  $Q$  is increased, and hence, both the temperature differences and the buoyancy force are augmented resulting in an increase in  $e^{++}$ .

Impacts of the nanofluid parameters ( $Nt$  and  $Nb$ ) on ratio of the average Nusselt number to the average Nusselt at the pure fluid  $Nu_m^+$  and ratio of the entropy generation ratio to the average Nusselt ratio at the pure fluid  $e^+$  are illustrated in Figs. 8(b), 9(a) and 9(b). The results revealed that  $Nu_m^+$  is diminished as the thermophores parameter  $Nt$  is increased, while the Brownian motion parameter  $Nb$  boosts values of  $Nu_m^+$ . Like effects of  $Nt$  on  $Nu_m^+$ , variations of  $Nt$  reduce values of  $e^+$ .

Figures 10(a) and 10(b) present profiles of ratio of the average Nusselt number to the average Nusselt at the pure fluid  $Nu_m^+$  under effects of the Hartmann number  $Ha$  and ratio of the entropy generation ratio to the average Nusselt ratio at the pure fluid  $e^+$  for different types of the nanofluids (Cu-water,  $Al_2O_3$ -water and hybrid nanofluid), respectively. It is found that  $Nu_m^+$  represents a decreasing function of  $Ha$  and  $\varphi$  parameters. In last, the results explored that dispersing  $Al_2O_3$  solid nanoparticles in the base fluid boosts values of  $e^+$ , whilst  $Al_2O_3$ -Cu nanoparticles give high values of  $e^+$  compared with classical nanofluids. Physically, dipping the hybrid nanoparticles within the non-Newtonian base fluid enhances the overall thermal conductivity of the mixture, and consequently, values of  $e^+$  are enhanced.

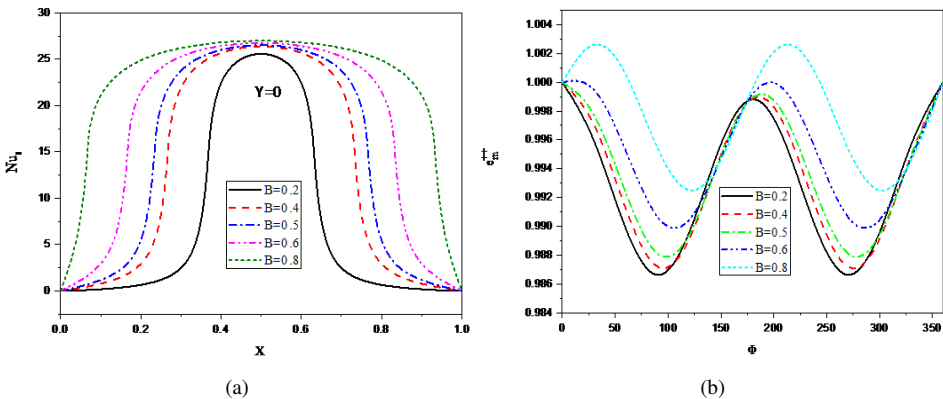


Figure 5. Profiles of (a)  $Nu_x$  and (b)  $e^{++}$  for lengths of the active parts  $B$ .

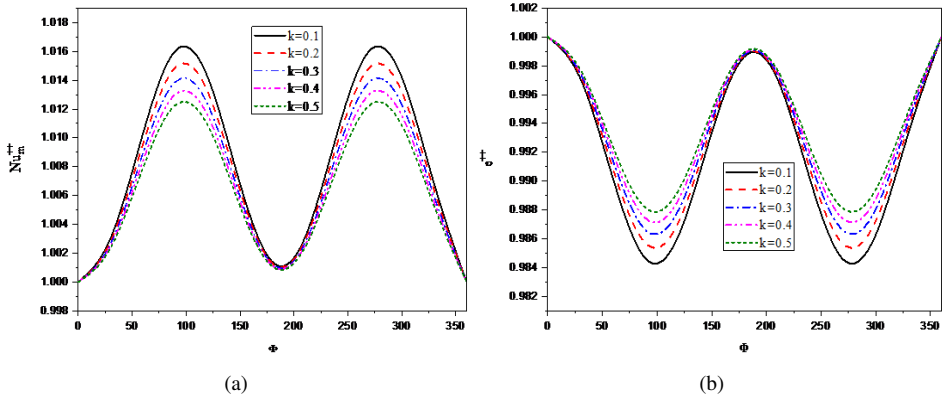


Figure 6. Profiles of (a)  $Nu_m^{++}$  and (b)  $e_c^{++}$  for the vortex viscosity  $k$ .

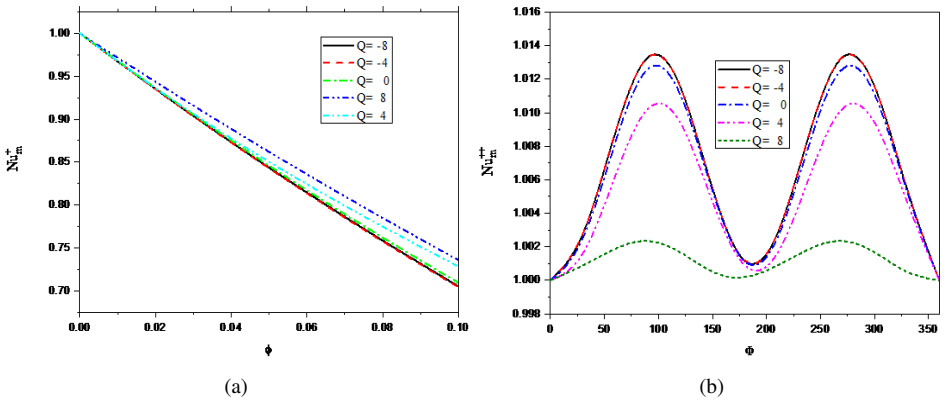


Figure 7. Profiles of (a)  $Nu_m^{++}$  and (b)  $Nu_m^{++}$  for the heat generation  $Q$ .

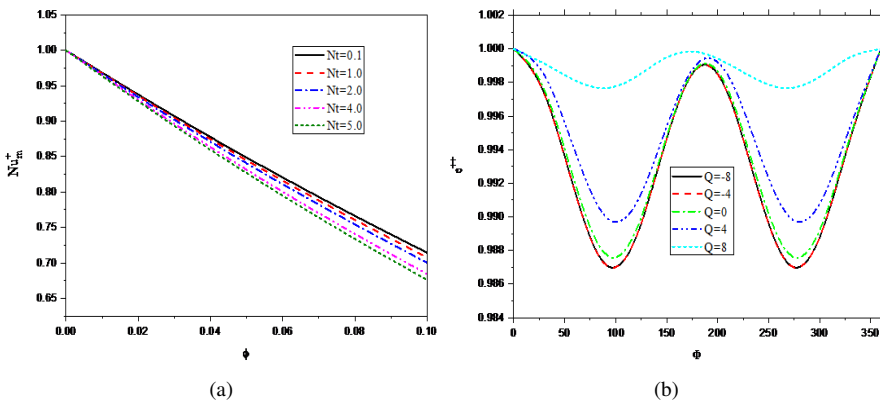


Figure 8. Profiles of (a)  $Nu_m^{++}$  for thermophoresis parameter  $Nt$ ; (b)  $e_m^{++}$  for the heat generation parameter  $Q$ .

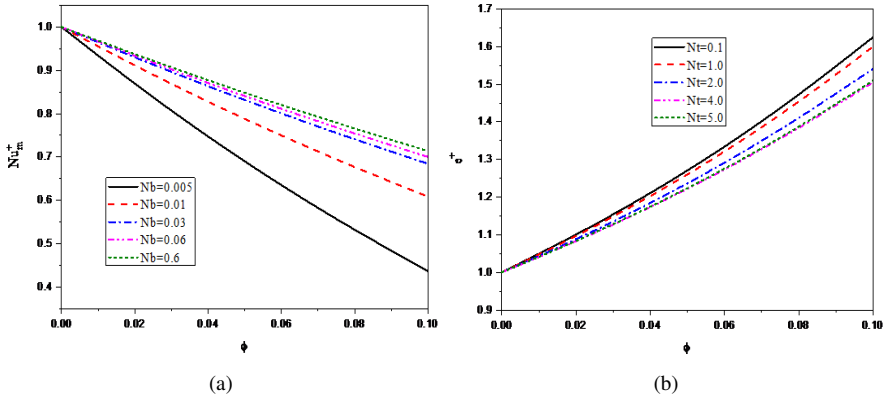


Figure 9. Profiles of (a)  $Nu_m^+$  for the Brownian parameter  $Nb$  and (b)  $e^+$  for thermophoresis parameter  $Nt$ .

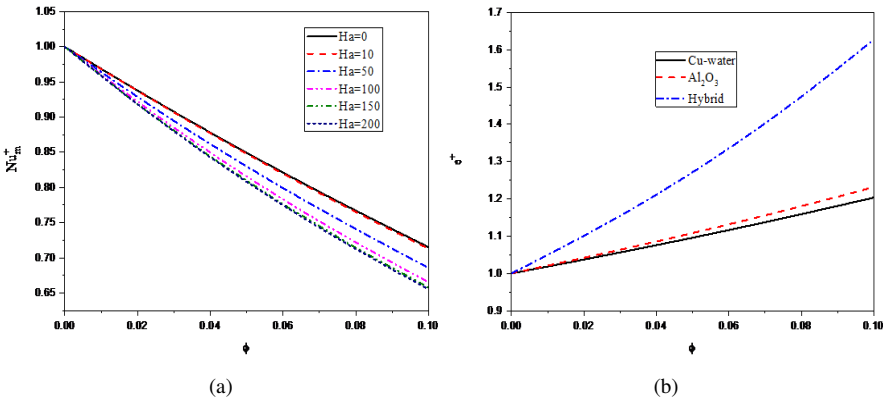


Figure 10. Profiles (a)  $Nu_m^+$  for the Hartmann number  $Ha$  and (b)  $e^+$  for the nanoparticles.

## 6 Conclusion

Numerical survey for the micropolar magnetic hybrid nanofluids flows within activated-walls enclosures filled by a porous medium was carried out. The entropy of the system was computed for wide variations of the governing parameter. Effects of an inclined electromagnetic force, heat generation/absorption and chemical reaction on features of the flows, angular velocity, heat and mass characteristics are examined. The worked mixture is consisting of water as a base fluid and copper as well as alumina as nanoparticles. The following outcomes are pointed out:

- (i) An increase in the vortex viscosity enhances the overall dynamic viscosity, and hence, the flow and ratio of the average Nusselt number to the average Nusselt number at a horizontal magnetic field are diminished.
- (ii) The decrease in the Darcy number decelerates the hybrid nanofluids motion, while the irreversibilities due to the thermal gradients are supported.

- (iii) The heated zones within the domain are reduced as lengths of the active parts are grown, while rate of the heat transfer is supported.
- (iv) Values of ratio of the average Nusselt number to the average Nusselt at the pure fluid  $Nu_m^+$  and ratio of the entropy generation ratio to the average Nusselt ratio to a horizontal magnetic field  $e^{++}$  are increased as the heat generation/absorption parameter is increased.
- (v) Ratio of the average Nusselt number to the average Nusselt to the pure fluid  $Nu_m^+$  is a decreasing function of the Hartmann number and nanoparticles volume fraction.
- (vi) Ratio of the entropy generation ratio to the average Nusselt ratio to the pure fluid  $e^+$  takes its maximum in case of hybrid nanofluids comparing with classical nanofluids.

## References

1. S.E. Ahmed, Non-Darcian natural convection of a nanofluid due to triangular fins within trapezoidal enclosures partially filled with a thermal non-equilibrium porous layer, *J. Therm. Anal. Calorim.*, **145**:1327–1340, 2020, <https://doi.org/10.1007/s10973-020-09831-4>.
2. S.E. Ahmed, M.A. Mansour, A. Mahdy, S.S. Mohamed, Entropy generation due to double diffusive convective flow of Casson fluids over nonlinearity stretching sheets with slip conditions, *Eng. Sci. Technol. Int. J.*, **20**(6):1553–1562, 2017, <https://doi.org/10.1016/j.jestch.2017.10.002>.
3. A. Bejan, *Entropy Generation Minimization*, 2nd ed., CRC, Boca Raton, FL, 1996.
4. H.C. Brinkman, The viscosity of concentrated suspensions and solutions, *J. Chem. Phys.*, **20**: 571, 1952, <https://doi.org/10.1063/1.1700493>.
5. S. Uma Devi, S.P.A. Devi, Numerical investigation of three-dimensional hybrid Cu-Al<sub>2</sub>O<sub>3</sub>/water nanofluid flow over a stretching sheet with effecting Lorentz force subject to Newtonian heating, *Can. J. Phys.*, **94**(5):490–496, 2016, <https://doi.org/10.1139/cjp-2015-0799>.
6. M. Famouri, K. Hooman, Entropy generation for natural convection by heated partitions in a cavity, *Int. Commun. Heat Mass Transfer*, **35**(4):492–502, 2008, <https://doi.org/10.1016/j.icheatmasstransfer.2007.09.009>.
7. T. Grosan, C. Revnic, I. Pop, D.B. Ingham, Magnetic field and internal heat generation effects on the free convection in a rectangular cavity filled with a porous medium, *Int. J. Heat Mass Transfer*, **52**(5–6):1525–1533, 2009, <https://doi.org/10.1016/j.ijheatmasstransfer.2008.08.011>.
8. G.G. Iliş, M. Mobedi, B. Sunden, Effect of aspect ratio on entropy generation in a rectangular cavity with differentially heated vertical walls, *Int. Commun. Heat Mass Transfer*, **35**:696–703, 2008, <https://doi.org/10.1016/j.icheatmasstransfer.2008.02.002>.
9. M.A. Ismael, T. Armaghani, A.J. Chamkha, Conjugate heat transfer and entropy generation in a cavity filled with a nanofluid-saturated porous media and heated by a triangular solid, *J. Taiwan Inst. Chem. Eng.*, **59**:138–151, 2016, <https://doi.org/10.1016/j.jtice.2015.09.012>.

10. G.H.R. Kefayati, Heat transfer and entropy generation of natural convection on non-Newtonian nanofluids in a porous cavity, *Powder Technol.*, **299**:127–149, 2016, <https://doi.org/10.1016/j.powtec.2016.05.032>.
11. G.H.R. Kefayati, Simulation of natural convection and entropy generation of non-Newtonian nanofluid in a porous cavity using Buongiorno's mathematical mode, *Int. J. Heat Mass Transfer*, **112**:709–744, 2017, <https://doi.org/10.1016/j.ijheatmasstransfer.2017.04.121>.
12. K. Khanafer, K. Vafai, M. Lightstone, Buoyancy-driven heat transfer enhancement in a two-dimensional enclosure utilizing nanofluids, *Int. J. Heat Mass Transfer*, **46**(19):3639–3653, 2003, [https://doi.org/10.1016/S0017-9310\(03\)00156-X](https://doi.org/10.1016/S0017-9310(03)00156-X).
13. B.S. Kim, D.S. Lee, M.Y. Ha, H.S. Yoon, A numerical study of natural convection in a square enclosure with a circular cylinder at different vertical locations, *Int. J. Heat Mass Transfer*, **51**(7–8):1888–1906, 2008, <https://doi.org/10.1016/j.ijheatmasstransfer.2007.06.033>.
14. H. Laouira, F. Mebarek-Oudina, A.K. Hussein, L. Kolsi, A. Merah, O. Younis, Heat transfer inside a horizontal channel with an open trapezoidal enclosure subjected to a heat source of different lengths, *Heat Transfer Asian Res.*, **49**:406–423, 2020, <https://doi.org/10.1002/htj.21618>.
15. D. Madhesh, R. Parameshwaran, S. Alaiselvam, Experimental investigation on convective heat transfer and rheological characteristics of Cu-TiO<sub>2</sub> hybrid nanofluids, *Exp. Therm. Fluid Sci.*, **52**:104–115, 2014, <https://doi.org/10.1016/j.expthermflusci.2013.08.026>.
16. M.A. Magherbi, A. Abbassi, A.B. Brahim, Entropy generation at the onset of natural convection, *Int. J. Heat Mass Transfer*, **46**(18):3441–3450, 2003, [https://doi.org/10.1016/S0017-9310\(03\)00133-9](https://doi.org/10.1016/S0017-9310(03)00133-9).
17. A. Mahdy, Simultaneous impacts of MHD and variable wall temperature on transient mixed Casson nanofluid flow in the stagnation point of rotating sphere, *Appl. Math. Mech.*, **39**(9):1327–1340, 2018, <https://doi.org/10.1007/s10483-018-2365-9>.
18. A. Mahdy, Entropy generation of tangent hyperbolic nanofluid flow past a stretched permeable cylinder: Variable wall temperature, *Proc. IMechE, Part E: J. Proc. Mech. Eng.*, **233**(3):570–580, 2019, <https://doi.org/10.1177/0954408918774898>.
19. A. Mahdy, M.A. Mansour, S.E. Ahmed, S.S. Mohamed, Entrop generation of Cu-water nanofluids through non-Darcy porous medium over a cone with convective boundary condition and viscous dissipation effects, *Spec. Top. Rev. Porous Media*, **8**(1):59–72, 2017, <https://doi.org/10.1615/SpecialTopicsRevPorousMedia.v8.i1.50>.
20. S. Mahmud, R.A. Fraser, Magnetohydrodynamic free convection and entropy generation in a square porous cavity, *Int. J. Heat Mass Transfer*, **47**:3245–3256, 2004, <https://doi.org/10.1016/j.ijheatmasstransfer.2004.02.005>.
21. S. Marzougui, F. Mebarek-Oudina, A. Assia, M. Magherbi, Z. Shah, K. Ramesh, Entropy generation on magneto-convective flow of copper-water nanofluid in a cavity with chamfers, *J. Therm. Anal. Calorim.*, **143**:2203–2214, 2021, <https://doi.org/10.1007/s10973-020-09662-3>.
22. J. Maxwell, *A Treatise on Electricity and Magnetism*, 2nd ed., Clarendon Press, Oxford, 1881.

23. F. Oueslati, B. Ben-Beya, T. Lili, Double-diffusive natural convection and entropy generation in an enclosure of aspect ratio 4 with partial vertical heating and salting sources, *Alex. Eng. J.*, **52**(4):605–625, 2013, <https://doi.org/10.1016/j.aej.2013.09.006>.
24. H.F. Oztop, E. Abu-Nada, Numerical study of natural convection in partially heated rectangular enclosures filled with nanofluids, *Int. J. Heat Fluid Flow*, **29**(5):1326–1336, 2008, <https://doi.org/10.1016/j.ijheatfluidflow.2008.04.009>.
25. A.M. Rashad, M.A. Mansour, T. Armaghani, A.J. Chamkha, MHD mixed convection and entropy generation of nanofluid in a lid-driven U-shaped cavity with internal heat and partial slip, *Phys. Fluids*, **31**:042006, 2019, <https://doi.org/10.1063/1.5079789>.
26. M.M. Rashidi, N. Kavyani, S. Abelman, Investigation of entropy generation in MHD and slip flow over a rotating porous disk with variable properties, *Int. J. Heat Mass Transfer*, **70**:892–917, 2014, <https://doi.org/10.1016/j.ijheatmasstransfer.2013.11.058>.
27. J. Raza, F. Mebarek-Oudina, P. Ram, S. Sharma, MHD flow of non-Newtonian molybdenum disulfide nanofluid in a converging/diverging channel with Rosseland radiation, *Defect Diffus. Forum*, **401**:92–106, 2020, <https://doi.org/10.4028/www.scientific.net/DDF.401.92>.
28. J. Sarkar, P. Ghosh, A. Adil, A review on hybrid nanofluids: Recent research, development and applications, *Appl. Math. Mech.*, **43**:164–177, 2015, <https://doi.org/10.1016/j.rser.2014.11.023>.
29. S.L. Sundar, M.K. Singh, A.C. Sousa, Enhanced heat transfer and friction factor of MWCNT-Fe<sub>3</sub>O<sub>4</sub>/water hybrid nanofluids, *Int. Commun. Heat Mass Transfer*, **52**:73–83, 2014, <https://doi.org/10.1016/j.icheatmasstransfer.2014.01.012>.
30. S. Suresh, K. Venkitaraj, P. Selvakumar, M. Chandrasekar, Synthesis of Al<sub>2</sub>O<sub>3</sub>-cu/water hybrid nanofluids using two step method and its thermo physical properties, *Colloids Surf., A*, **388**:41–48, 2011, <https://doi.org/10.1016/j.colsurfa.2011.08.005>.
31. B. Takabi, S. Salehi, Augmentation of the heat transfer performance of a sinusoidal corrugated enclosure by employing hybrid nanofluid, *Adv. Mech. Eng.*, **6**:147059, 2014, <https://doi.org/10.1155/2014/147059>.
32. T. Tayebi, A.J. Chamkha, Free convection enhancement in an annulus between horizontal confocal elliptical cylinders using hybrid nanofluids, *Numer. Heat Transfer, Part A*, **70**(10):1141–1156, 2016, <https://doi.org/10.1080/10407782.2016.1230423>.